ELSEVIER

Colloids and Surfaces A: Physicochem. Eng. Aspects 255 (2005) 19–25

COLLOIDS AND SURFACES A

www.elsevier.com/locate/colsurfa

Magnetic enhancement of iron oxide nanoparticles encapsulated with poly(D,L-latide-co-glycolide)

Seung-Jun Lee[a], Jong-Ryul Jeong[b], Sung-Chul Shin[b], Jin-Chul Kim[c], Young-Hwan Chang[d], Kwon-Hyung Lee[a], Jong-Duk Kim[a,*]

[a] *Department of Chemical and Biomolecular Engineering, Center for Ultramicrochemical Process Systems, KAIST, Daejeon 305-701, Republic of Korea*
[b] *Department of Physics, Center for Nanospinics of Spintronic Materials, KAIST, Daejeon 305-701, Republic of Korea*
[c] *School of Biotechnology and Bioengineering, Kangwon National University, Chunchon 200-701, Republic of Korea*
[d] *Division of Natural Science, KAIST, Daejeon 305-701, Republic of Korea*

Received 2 September 2004; accepted 7 December 2004
Available online 18 January 2005

Abstract

Iron oxide nanoparticles encapsulated (II) with poly(D,L-lactide-co-glycolide) (PLGA) having high magnetic susceptibility were prepared by an emulsification–diffusion method. The preparation method consists of emulsifying an aqueous solution of PLGA in ethylacetate and extracting the organic solvent into a water phase. After mutual saturation of the organic and the continuous phases, PLGA precipitated to encapsulate nanoparticles (I) by adding excess water. As the homogenization strength in the emulsification step and the agitation speed in the solvent diffusion step increased, the mean size of IONE (iron oxide nanoparticles encapsulated) was reduced to a limiting size. The images under SEM and TEM showed that IONE has almost a spherical shape with 90–180 nm and that iron oxide nanoparticles with 8–20 nm were embedded in the PLGA matrix. The magnetization of IONE was measured with vibrating sample magnetometer (VSM), varying the size from 120 to 180 nm. It is observed that the small IONEs have a high magnetic susceptibility. It is attributed that the packing densities of iron oxide nanoparticles and IONE increased as their sizes decreased.

Keywords: Nanoparticles; Encapsulation; Emulsification–diffusion method; Magnetite; Iron oxide

1. Introduction

Functionalized magnetic nanoparticles are used in several biomedical applications, such as drug delivery, magnetic cell separation and magnetic resonance imaging (MRI) contrast agent for diagnostics. Magnetic composite particles with polystyrene [1], polyethylene [2], or polyacrylic acids [3] have been reported earlier for magnetic O-ring lubricating seals and in non-destructive evaluation. In biomedical fields, meanwhile, iron oxide nanoparticles are used in both diagnostics, e.g. contrast agent medium in radiological imaging techniques [4] or specific cell separation [5], and therapeutic regimes, such as embolization of aneurysms with an external magnetic field [6,7] or the development of an implantable artificial heart [8]. Iron oxide nanoparticles have also been the subject of much fundamental research as a magnetic resonance imaging (MRI) contrast agent [9].

Polymeric nanocapsules for a site-specific drug delivery [16] were fabricated using water-in-oil-in-water (w/o/w) emulsion systems in a form of albumin and starch microspheres, poly(alkyl-cyanoacrylate) nanoparticles, magnetic emulsion, liposomes, and magnetic granula [10]. However, therapeutic experiments of magnetic particles were limited in animals [11–13], but one case in human beings suffering from untreatable cancer disease was undertaken using an intravenous injection [14,15]. Thereafter, much interest has focused on the use of particles prepared with poly(D,L-lactide-co-glycolide) (PLGA), poly(D,L-lactide) (PLA), and poly(glycolide) (PGA). These polyesters have biocompatible

* Corresponding author. Tel.: +82 42 869 3961; fax: +82 42 869 3910.
E-mail address: jdkim@kaist.ac.kr (J.-D. Kim).

0927-7757/$ – see front matter © 2004 Elsevier B.V. All rights reserved.
doi:10.1016/j.colsurfa.2004.12.019

and biodegradable properties and low toxicity, and approved by FDA [19,20]. Their degradation could be controlled by molecular weight, crystallinity, and the ratio of lactide to glycolide [17,18].

In this study, nanocapsules containing PLGA and iron oxides nanoparticles were prepared by an emulsification–diffusion technique [21]. The encapsulation process involves the formation of a conventional oil-in-water emulsion which consists of an oil phase containing a partially water-miscible solvent, matrix polymer and iron oxide nanoparticles, and an aqueous phase containing a stabilizer. The subsequent addition of oil phase into aqueous media forms an oil-in-water-type emulsion and then the solvent diffuses out and dissolves at the external phase. The morphologies of nanocapsules thus prepared were investigated with the process variables such as the concentrations of polymer, and the mixing degree of emulsion system. Their magnetic properties of resulting nanocapsules were also examined.

2. Experimental methods and characterization

2.1. Materials

Poly(D,L-lactide-co-glycolide) (PLGA) with a weight–average molecular weight of 75,000–120,000 and D,L-lactide to glycolide ratio of 75:25 was purchased from Sigma (St Louis, MO). Iron oxide nanoparticles of 8–20 nm (Ferrofluid W-40, magnetic content 40%, Taiho Industries Co. Ltd., Tokyo, Japan) (I) was used as a core material. Pluonic F-127 (poloxamer 407, nonionic) and Pluonic F-68 (poloxamer 188, nonionic) were purchased from Sigma Chemical Co. Ethyl acetate (EtAc, Fluka) was used as a partially water-miscible solvent. Distilled water was of Milli-Q quality (Millipore, USA-Bedford, MD). All organic solvents were either HPLC grade or American Chemical Society analytical grade reagents.

2.2. Encapsulation of nanoparticles with PLGA

Iron oxide nanoparticles were encapsulated with PLGA (IONE) (II) by using an emulsification–diffusion method. A schematic diagram of the process is shown in Fig. 1.

In brief, 150 mg of PLGA was dissolved in 10 ml of ethylacetate (density, 0.9003 g/cm^3 at 20 °C) and 2 wt.% of polymer solution was formed. Then, 5 mg of Ferrofluid W-40 (magnetic contents, 40%) (I) was added. The mixture was sonicated for 5 min with a bath-type sonicator (Soncis and Material, Danbury, CT). The organic mixture with iron oxide nanoparticles (I) was added into 20 ml of an aqueous phase containing a 5% of Pluonic F-127. After mutual saturation of organic mixture and continuous phases, the mixture was emulsified for 7 min with a high-speed homogenizer (about 8000–24,000 rpm), and then an excess amount of water is added to the o/w emulsion under sonication. The subsequent addition of water dilutes the solvent concentration in water and extracts solvent from the organic solution, leading to the nanoprecipitation of polymer matrix entrapped with ion oxide nanoparticles. The relative viscosity of the o/w emulsion, and the ratio of solution to solvent viscosity, determined using Cannon-Fenske Viscometer (Made in Korea Dong-Jin Instrument Corp., Capillary No. 150) were used for the dispersion properties of emulsions.

2.3. Characterization of iron oxide nanoparticle (I) and IONE (II)

The microscopic images of iron oxide nanoparticles (I) and IONE (II) were observed on TEM (Philips Model CM 20) and SEM (Philips Model XL 308FEG). For TEM images,

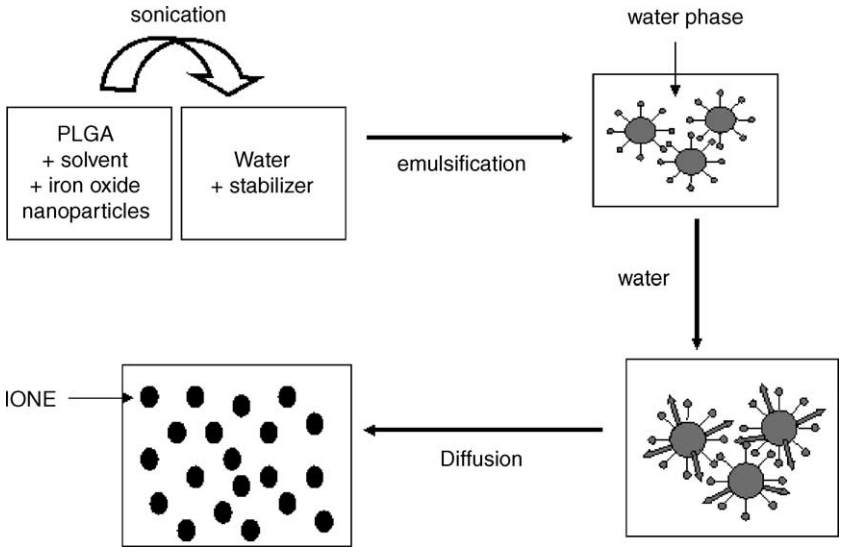

Fig. 1. Schematic representation a process for the preparation of the iron oxide nanoparticles encapsulated (IONE) (II).

a drop of a dilute dispersion was deposited on a copper grid covered with a formal-carbon membrane. An X-ray diffraction measurement was performed to identify the crystal structure of iron oxide nanoparticles (Rigaku D/max-rc(12 kw)). The particle size of encapsulated nanoparticles IONE (II) was determined by a dynamic light scattering method (Zeta plus, Brookhaven Inst. Co., USA). For analysis, 0.5 ml of IONE suspension was diluted to 5 ml with D.D.I. water. Measurements were made in a triplicate for each sample. Magnetization measurements of both iron oxide nanoparticle (I) and IONE (II) were performed at room temperature using a vibrating sample magnetometer (VSM). When a sample is placed in a uniform magnetic field, it undergoes a sinusoidal motion (i.e. mechanical vibration), and thus a significant magnetic flux change is developed. This change induces a voltage in the pick-up coils, which is proportional to the magnetic moment of the sample. To investigate the magnetic properties of PLGA-encapsulated magnetic nanoparticles, FC/ZFC measurements have been made using an SQUID magnetometer.

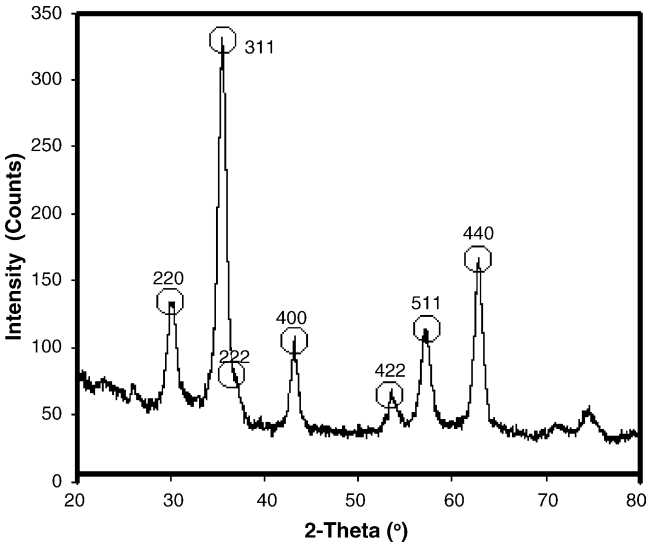

Fig. 3. X-ray diffraction pattern of iron oxide nanoparticles nanocrystallites (I).

3. Results and discussions

3.1. Characteristics of iron oxide nanoparticles

Ferrofluid is a colloid of magnetite particles in an aqueous phase [22] and the surface of magnetite particles was coated first with a monolayer of sodium oleate by strong chemisorption and then with a monolayer of sodium dodecylbenzenesulfonate (SDBS) by weak physisorption. The aqueous phase contains a large amount of SDBS as a stabilizer. TEM micrograph in Fig. 2 shows that iron oxide nanoparticles (I) were apparently spherical and 8–20 nm in size. X-ray diffraction measurement was performed to identify the crystallographic structure of iron oxide nanoparticles and presented in Fig. 3.

The well-defined X-ray diffraction pattern indicates the formation of highly crystallized iron oxide The XRD measurement, which was performed to identify the crystallographic structure of iron oxide nanoparticle, revealed peaks characteristic of magnetite Fe_3O_4 (Fe_3O_4, Powder Diffraction file, JCPOS 19-0629). Magnetization curves, obtained at room temperature from the dried iron oxide nanoparticles (I), shows a superparamagnetic behavior in Fig. 4.

3.2. Encapsulation of iron oxide nanoparticle

The process of encapsulating nanoparticles by the emulsification–diffusion method (Fig. 1) consists of two steps: emulsification and diffusion. After dispersing iron ox-

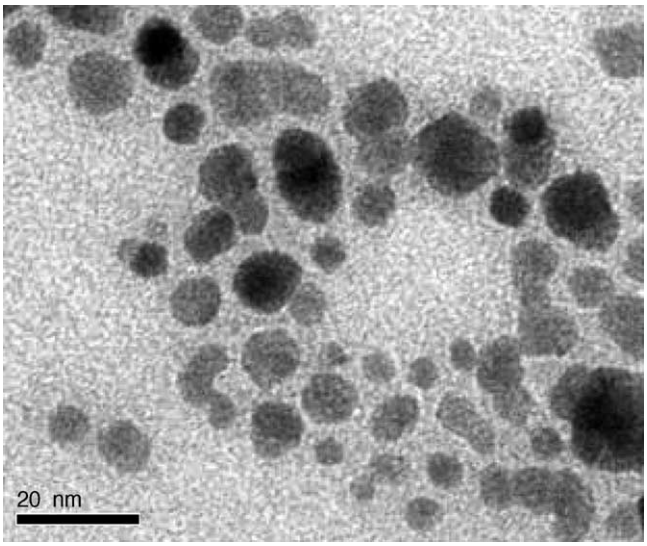

Fig. 2. Transmission electron microscopy of iron oxide nanoparticles (I).

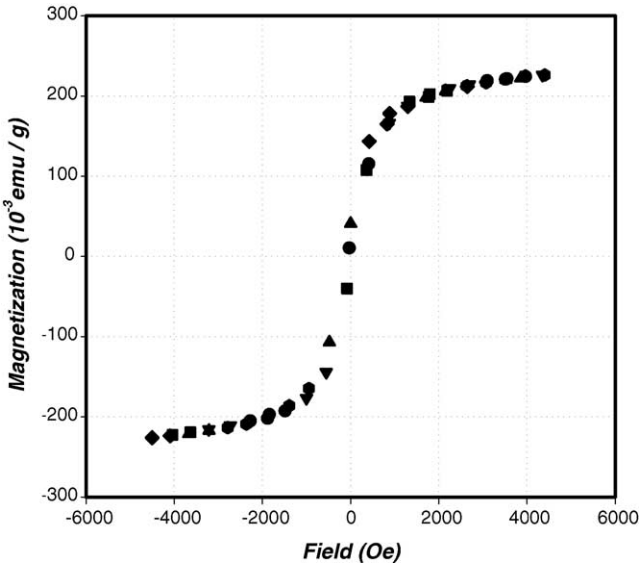

Fig. 4. Hysteresis plot of the magnetization of iron oxide nanoparticles (I).

Table 1
Effect of homogenizer speed on the viscosity of emulsion and the Reynolds number

Type	V_{im}[a]	η_{rel}[b]	μ_{em}[c]	N_{Re}[d]
I	8000			1430
		5.8 ± 0.03	5.7 ± 0.05	
II	13500			3860
		3.6 ± 0.05	3.6 ± 0.01	
III	17000			5860
		3.0 ± 0.02	2.9 ± 0.03	
IV	20000			7700
		2.7 ± 0.01	2.6 ± 0.06	
V	24000			9400

[a] The rotational velocity of impellar (rpm).
[b] Relative viscosity (η/η_0).
[c] The viscosity of emulsion (cp).
[d] Reynolds number ($Re = \rho_{vd}/\mu$).

ide nanoparticles (I) in an ethylacetate solution of PLGA, the dispersion was emulsified in an aqueous solution of 5% Pluonic. PLGA concentrations were varied from 0.5 to 5.0% (w/v). The solubility of ethylacetate is about 10% in water and therefore, the volume ratio of ethylacetate to water must be at least smaller than 1/10 in the final form of emulsion.

3.2.1. The effect of rotational velocity

Droplets must be deformed by the viscous stress τ exerted by the surrounding liquid, and disrupted to form small droplets if the stress overcomes the Laplace pressure generated by the formation of curvature. When the diameter of impellar of homogenizer (D_I) is 1.0 cm, and the density of emulsion (ρ_{em}) is 1.03 g/cm^3, Reynolds number of fluid in homogenizer ($Re = D_I V_{im} \rho_{em}/\mu_{em}$) at 8000 rpm was 1430 and those at higher rpm were given at the Table 1, where the rotational velocity of impellar V_{im} is in cm/s and the viscosity of emulsion μ_{em} is in g/cm s. Since the Reynolds number indicates (inertial force provided be impellar)/(viscous force), it is convenient to choose a variable, V_{im} as an operating one.

As the homogenizer speed increases, the high shear stress develops to reduce the size of droplets and finally the size of IONE (II). The interfacial stability can be determined by the balance between tangential stress at interface ($\mu G_0 = \mu(dU_z/dy)_{y=0}$) and the interfacial tension gradient $-(d\gamma/dz)_{y=0}$, where $y = 0$ is the locus of interface and z is the tangential direction at interface. The impact of rotating impellar is stretching the interface, while the gradient of interfacial tension generated thus can be dissipated by the molecular diffusion of interfacial materials. Therefore, if the former is greater, the layer will be stretched, continuously forming small droplets, but if the latter is greater, the surface area will be rapidly reduced to form large droplets. In addition, the viscoelastic properties of polymer solutions would be also responsible for highly susceptible droplets from the deformation given by the mechanical impact. Further, the homogenizer speed affects the relative viscosity (η_{rel}) of emulsion as shown in Table 1. In order to prepare fine particles, it seems to be critical to reduce the effective viscosity of emulsions (see

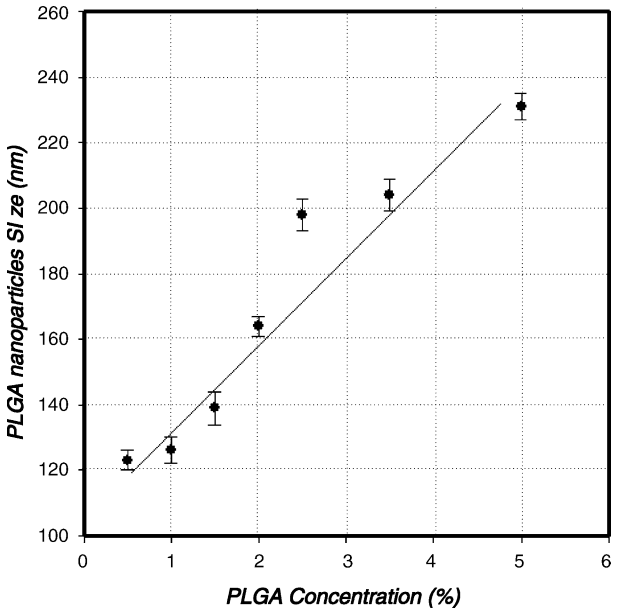

Fig. 5. The effect of homogenization speeds in the emulsification step on the size of the iron oxide nanoparticles encapsulated (IONE) (II).

Fig. 5 and Table 1). The viscosity reduction at a higher speed may indicate the transition from coarse to fine droplets in the Stokes regime. However, as the emulsion droplets are reduced further, the friction loss of kinetic velocity of droplets increases. Therefore, shear stress would reduce the size of droplets and finally the viscosity of oil-in-water phase unchanged in a saturated manner. Fig. 5 and Table 1 show the mean particle size and the relative viscosity of emulsion with increasing rotational speed. The mean particle size of IONE was found to decrease up to 120 from 200 nm as homogenizer speed increased. The effect of agitation speed on the particle size has also been studied in the diffusion step (Fig. 6). The mean diameter decreased from 115 to 90 nm and no further decrease was observed at a higher speed. Both steps of oil-in-water droplets formation and the solvent diffusion into the aqueous phase were found to control the size and its distribution of IONE (II).

In a homogenizer and an agitator, the rotational velocity of shaft (rpm) determines the droplet size and the fluid mechanical behaviors of emulsions. It is expected that the high speed may reduce the droplet size and in fact the coating layer and the emulsion viscosity μ_{em} or transform the multiparticle core to monocore capsules.

3.2.2. The effect of PLGA concentration

During the homogenization period, the degree of emulsification was intense and short enough to break the oil phase into small droplets, while the agitation speed of the diffusion step is mild and sustained so as to maintain the droplets stable without coalescence and enhance the ethylacetate diffusion into water. When EtAc diffuses from the polymer solution into the water, a polymer layer forms near the interface as

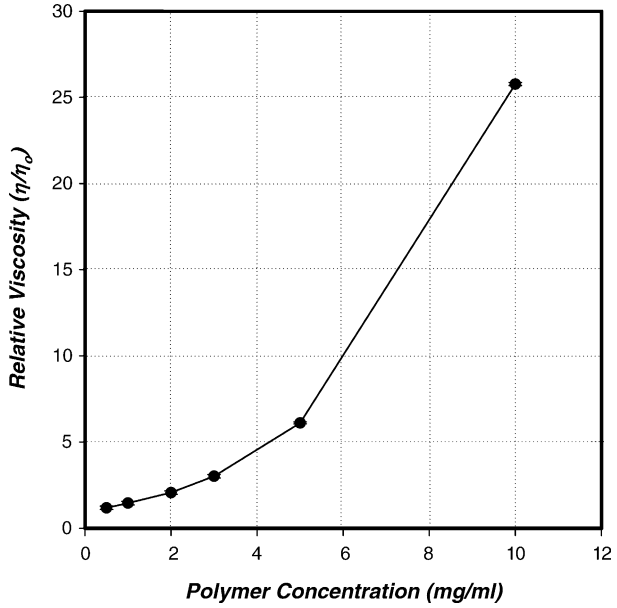

Fig. 6. The effect of agitator speeds in the solvent diffusion step on the size of the iron oxide nanoparticles encapsulated (IONE) (II).

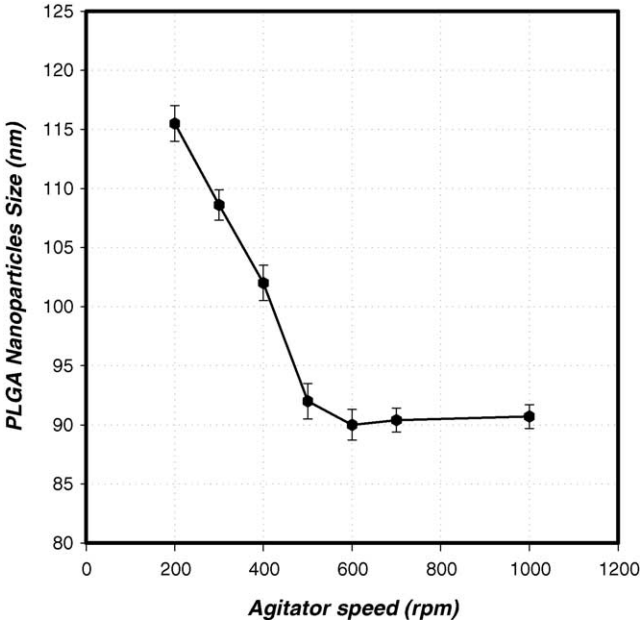

Fig. 8. The effect of PLGA concentrations on the relative viscosity.

if it forms a nanocapsule. Fig. 7 shows the effect of PLGA polymer concentration on the particle size of IONE (II). As the PLGA concentration in the internal phase increases, the size of IONE (II) increased in agreement with others [17]. The increase of PLGA concentrations indicates the increase of viscosities of polymer solutions. It is because the high viscosity provides the resistance to the shear forces and restricts the formation of nanoparticles. Fig. 8 shows the effect of PLGA polymer concentration on the relative viscosity through Cannon–Fenske Viscometer (Made in Korea Dong-Jin Instrument Corp., Capillary no 150). In this study, IONE size was affected by three factors, homogenizer speed, agitator speed, and PLGA concentration. Therefore the value of the other two factors fixed to investigate the influence of one factor for preparation of IONE was shown in Table 2.

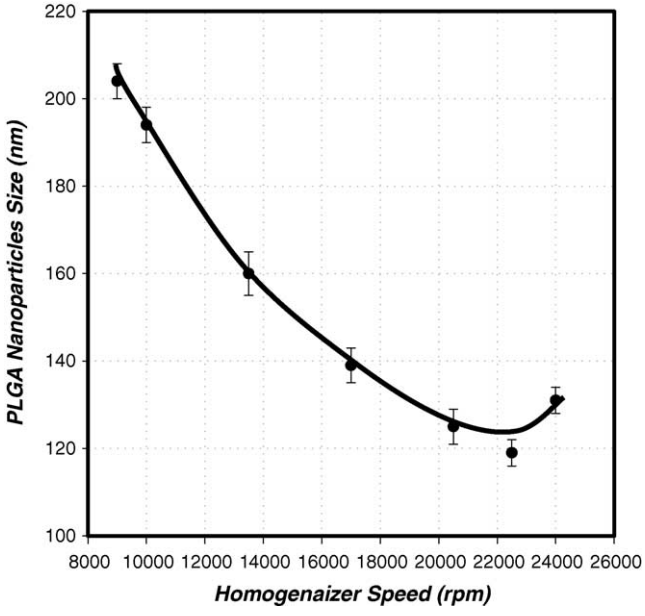

Fig. 7. The effect of PLGA concentrations on the size of the iron oxide nanoparticles encapsulated (IONE) (II).

3.2.3. *The structure and morphology*

The structure and morphology of IONE (II) were observed by TEM and SEM. Fig. 9(a) showed that structure of IONE prepared at 22,000 rpm with the o/w ratio of 1:2. The nanoparticles encapsulated in PLGA can be seen as dark domains. As shown, the ferrite particles (I) were entrapped in IONE (II) but the nanocapsules contain more than one nanoparticles (I). Fig. 9(b) showed the morphology of IONEs. They were almost spherical. Also, a convex region in the surface of IONEs is observed where it was coated with gold nanoparticles of 10 nm for protecting sample before measuring SEM.

3.3. *Effect of magnetization susceptibility*

The magnetization of IONE (II) on the capsule size is shown in Fig. 10. As the size of IONE decreased, the mag-

Table 2
The value of the other two factors fixed for the preparation of IONE

	Polymer concentration	Homogenizer speed	Agitator speed
Fig. 5	Variable	15000 rpm	400 rpm
Fig. 7	20 mg/ml	Variable	400 rpm
Fig. 8	20 mg/ml	20000 rpm	Variable

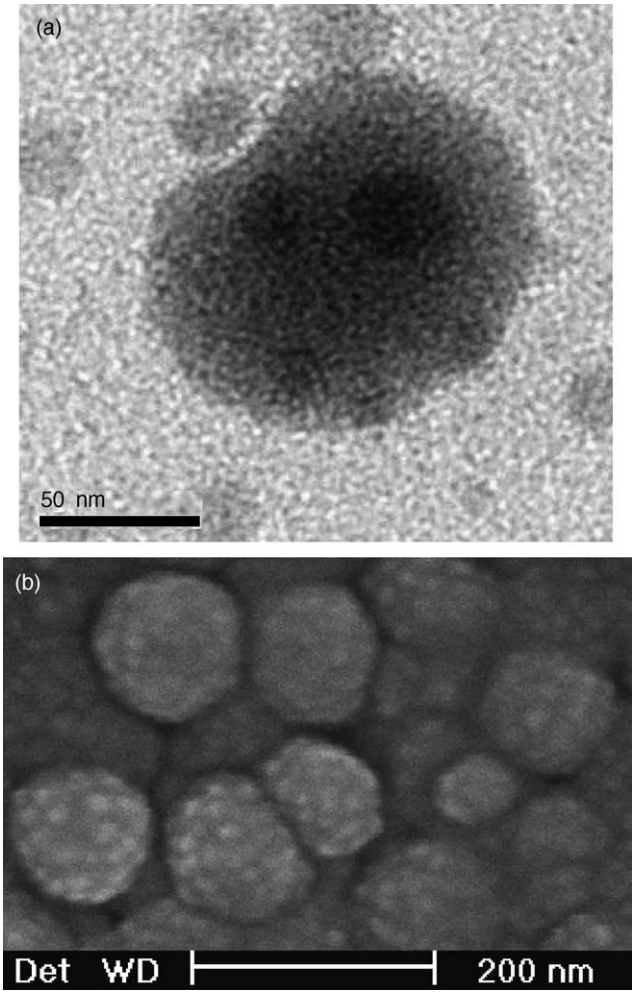

Fig. 9. Electron micrographs of the iron oxide nanoparticles encapsulated (IONE) (II): (a) transmission electron micrograph; (b) scanning electron micrograph.

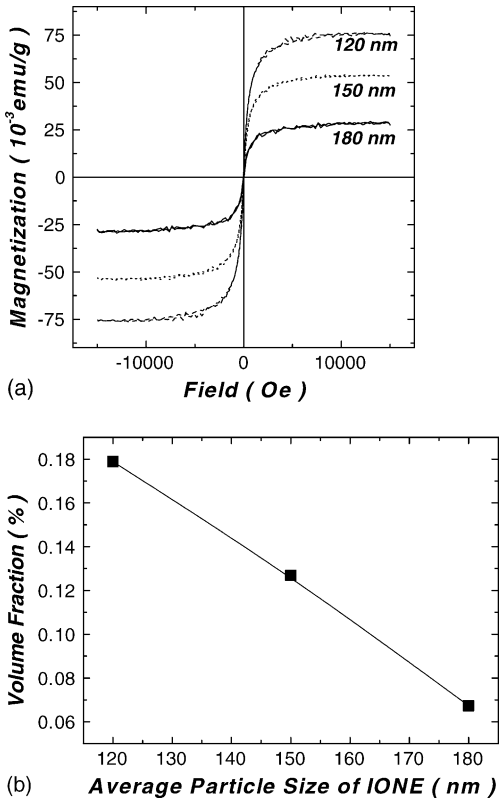

Fig. 10. (a) The effect of magnetic susceptibility of IONE (II) as the particle size; (b) the influence of the volume fraction as the size of IONE.

netic susceptibility increased as shown in Fig. 10(a). It is apparently related to the volume fraction of nanoparticles (I) which increase at small nanocapsules in the Fig. 10(b). The tight packing of nanoparticles (I) in nanocapsules increases the particle density of ferrite and thus increases the saturation magnetization. To investigate the magnetic properties of PLGA-encapsulated magnetic nanoparticles, FC/ZFC measurements have been made using an SQUID magnetometer. Fig. 11 shows the FC and ZFC curves for the 120 nm PLGA-encapsulated nanoparticles from 5 to 300 K at 200 Oe. The ZFC and FC curves are coincided above 175 K and separated below 175 K. The ZFC curve shows a broad peak at $T_{max} \sim 125 \pm 10$ K indicative of a characteristic blocking temperature for superparamagnetic particles [23–25]. It is well known that the broad peak in ZFC curve generally implies the distribution in particle size and anisotropy of nanoparticles [26]. For the samples of PLGA-encapsulated magnetic nanoparticles, the broad peak around $T_{max} = 125 \pm 10$ K could be ascribed to wide size distribution caused by clustering between embedded iron oxide nanoparticles in PLGA matrix. As shown in the inset of Fig. 10, TEM study revealed that the size of agglomerated magnetic nanoparticles is ranged from 10–80 nm. The details of magnetic properties of them were described in a previous paper [27].

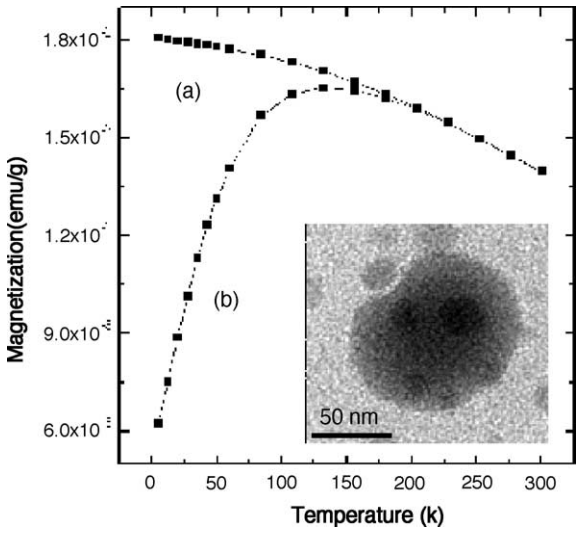

Fig. 11. Temperature dependence of the magnetization curves of IONE (II) under (a) FC and (b) ZFC at 200 Oe. The inset shows TEM image of magnetic nanoparticles embedded in the PLGA polymer matrix.

4. Conclusion

The magnetic enhancement of iron oxide nanocapsules IONE (II) have been achieved when iron oxides nanoparticles (I) were encapsulated by emulsification–diffusion technique. The process variables such as the homogenization strength in the emulsification step and the agitation speed in the diffusion step were investigated to control the size of IONE (II). It was observed that the dominating factors to control the size were the homogenization strength and the optimal polymer concentration. Magnetic susceptibility of IONE (II) increases as the size of IONE (II) decreases. It is attributed that the packing density or volume fraction of nanoparticles increased as the size of IONE decreased.

Acknowledgements

This research is partially supported by Center for Ultramicrochemical Process Systems project and by the Korean Ministry of Science and Technology through Strategic National R&D program and the Creative Research Initiatives Project.

References

[1] X. Xu, G. Friedman, et al., Chem. Mater. 14 (2002) 1249.
[2] J. Chatterjee, Y. Haik, et al., J. Magn. Magn. Mater. 246 (2002) 382.
[3] P.A. Dresco, S.Z. Vladimir, R.J. Gambini, C. Benjamin, Langmuir 15 (1999) 1945.
[4] R. Weissleder, P.F. Hahn, D.D. Stark, et al., Am. J. Roentgenol. 149 (1987) 723.
[5] J.E. Hardingham, D. Kotask, R.E. Sage, et al., Mol. Med. 1 (1995) 789.
[6] J.E. Alksne, A. Fingerhut, R. Rand, Surgery 60 (1966) 212.
[7] S.K. Hilal, W.J. Michelsen, J. Driller, E. Leonard, Radiology 113 (1974) 529.
[8] Y. Mitamura, T. Wada, S. Keisuke, Artif. Organs 16 (1992) 490.
[9] Q.T. Bui, Q.A. Pankhurst, et al., IEEE Trans. Magn. 34 (1998) 4.
[10] P.K. Gupta, C.T. Hung, in: N. Willmott, J. Daly (Eds.), Microspheres and Regional Cancer Therapy, CRC Press, Boca Raton, FL, 1994, p. 71.
[11] A.S. Lubbe, C. Bergemann, J. Brock, D.G. McClure, J. Magn. Magn. Mater. 194 (1999) 149.
[12] P.K. Gupta, C.T. Hung, J. Microencap. 7 (1990) 85.
[13] U.O. Hafeli, G.J. Pauer, W.K. Roberts, et al., in: U.O. Hafeli, W. Schutt, J. Teller, M. Zborowski (Eds.), Scientific and Clinical Application of Magnetic Carriers, Plenum press, New York, 1996, p. 501.
[14] A.S. Lubbe, C. Bergemanm, H. Riess, et al., Cancer Res. 56 (1996) 4686.
[15] C. Alexiou, P. Hulin, et al., J. Magn. Magn. Mater. 225 (2001) 187.
[16] D. Quintanat-Guerrero, E. Allemann, E. Doelker, H. Fessi, Pharmaceut. Res. 15 (1998) 1056.
[17] H.Y. Kwon, J.Y. Lee, S.W. Choi, J.H. Kim, Colloid Surf. A 182 (2001) 123.
[18] D. Lemoine, C. Francois, F. Kedzierewicz, V. Preat, M. Hoffman, P. Maincent, Biomaterials 17 (1996) 2191.
[19] J. Herrman, R. Bodmeier, Biodegradable somatostatin acetate containing microspheres prepared by various aqueous and non-aqueous solvent evaporation technique, Eur. J. Pharm. 45 (1998) 75.
[20] Y.S. Lin, T.L. Ho, L.H. Chiou, Microencapsulation and controlled release of in sulin from polylactic acid microcapsules, Med. Devices Art. Org. 13 (1986) 187.
[21] D. Quintanar-Guerrero, E. Allemann, E. Doelker, H. Fessi, Colloid Polym. Sci. 275 (1997) 640.
[22] (a) J. Shimoiizaka, K. Nakatsuka, Hyomen 13 (1975) 103;
(b) J. Shimoiizaka, K. Nakatsuka, R. Chubachi, Y. Sato, Stabilization of aqueous magnetite suspension, Nippon Kagaku Kaishi 8 (1) (1976) 6–9.
[23] B.H. Sohn, R.E. Cohen, G.C. Papaefthymiou, J. Magn. Magn. Mater. 182 (1998) 216.
[24] D.K. Kim, Y. Zhang, W. Voit, K.V. Rao, M. Muhammed, J. Magn. Magn. Mater. 225 (2001) 30.
[25] L. Zhang, G.C. Papaefthymiou, J.Y. Ying, J. Phys. Chem. B 105 (2001) 7414.
[26] B.D. Cullity, Introduction to Magnetic Materials, Addison-Wesley, Massachusetts, 1972, pp. 410–418.
[27] (a) J.-R. Jeong, S.-J. Lee, J.-D. Kim, S.-C. Shin, IEEE Trans. Magn. 40 (2004) 3015;
(b) J.-R. Jeong, S.-J. Lee, J.-D. Kim, S.-C. Shin, Phys. Stat. Sol. B 241 (2004) 1593.